Plasmonic Green Nanolaser Based on a Metal-Oxide-Semiconductor Structure

ARTICLE *in* NANO LETTERS · SEPTEMBER 2011

Impact Factor: 13.59 · DOI: 10.1021/nl2022477 · Source: PubMed

NANO LETTERS

LETTER

pubs.acs.org/NanoLett

Plasmonic Green Nanolaser Based on a Metal−Oxide−Semiconductor Structure

Chen-Ying Wu,[†] Cheng-Tai Kuo,[†] Chun-Yuan Wang,[†] Chieh-Lun He,[‡] Meng-Hsien Lin,[‡] Hyeyoung Ahn,[*,§] and Shangjr Gwo[*,†,‡]

[†]Department of Physics and [‡]Institute of Nanoengineering and Microsystems, National Tsing-Hua University, Hsinchu, Taiwan 30013, Republic of China

[§]Department of Photonics and Institute of Electro-optical engineering, National Chiao-Tung University, Hsinchu, Taiwan 30010, Republic of China

Supporting Information

ABSTRACT: Realization of smaller and faster coherent light sources is critically important for the emerging applications in nanophotonics and information technology. Semiconductor lasers are arguably the most suitable candidate for such purposes. However, the minimum size of conventional semiconductor lasers utilizing dielectric optical cavities for sustaining laser oscillation is ultimately governed by the diffraction limit ($\sim(\lambda/2n)^3$ for three-dimensional (3D) cavities, where λ is the free-space wavelength and n is the refractive index). Here, we demonstrate the 3D subdiffraction-limited laser operation in the green spectral region based on a metal−oxide−semiconductor (MOS) structure, comprising a bundle of green-emitting InGaN/GaN nanorods strongly coupled to a gold plate through a SiO_2 dielectric nanogap layer. In this plasmonic nanocavity structure, the analogue of MOS-type "nanocapacitor" in nanoelectronics leads to the confinement of the plasmonic field into a 3D mode volume of 8.0×10^{-4} μm^3 ($\sim 0.14(\lambda/2n)^3$).

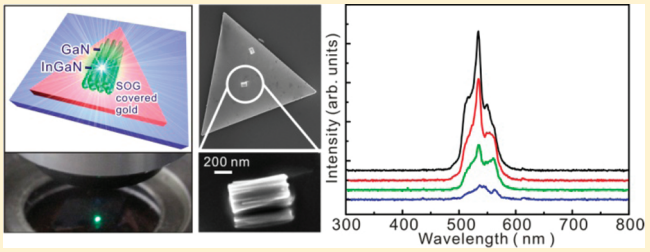

KEYWORDS: Plasmonic nanolaser, surface plasmon polariton, indium gallium nitride, nanorod

The key to achieving the most compact footprint for semiconductor lasers is the miniaturization of their resonant cavities. In the past two decades, various types of semiconductor cavity structures have been demonstrated for this purpose, including microdisks,[1] nanowires,[2−5] and photonic crystal nanocavities.[6−8] However, most of these approaches only focus on reducing cavity sizes in one[1] or two dimensions[2−5] due to the adverse effects of cavity size reduction on lasing threshold. For the case of photonic crystal nanocavities with ultrasmall optical mode volumes, their physical sizes remain large (many wavelengths) in order to maintain high cavity finesse. To date, reducing the physical size of semiconductor laser cavities in all three dimensions, while maintaining a manageable lasing threshold, stands as the ultimate challenge in realizing subwavelength semiconductor nanolasers.[9−11]

The recent advent of nanoplasmonics based on metallodielectric structures has brought a large-scale paradigm shift in designing optical components and optoelectronic devices in the deep subwavelength regime.[12−15] Especially, a new class of lasers based on surface plasmon amplification by stimulated emission of radiation (spaser) has been proposed[16−18] and demonstrated[19−22] as the source and amplifier of coherent optical and surface plasmon fields. In the subdiffraction-limited spaser operation, surface plasmons excited in noble-metal structure adjacent to gain medium provide the necessary coherent feedback. In metal-cladded dielectric nanocavities,[10,11] it has recently been found that metals can suppress leaky optical modes and alleviate the issue of cross-coupling in closely packed cavity arrays. In particular, for noble metals such as gold and silver, the surface plasmon polariton (SPP) resonant modes in the visible region allows for novel schemes to confine the light field into a deep subwavelength plasmonic nanocavity. However, the metallic nanocavity typically exhibits both high Ohmic (Joule) and radiation losses. As a result, the spasing threshold for nanolasers based on plasmonic cavities could be very high.

To overcome the difficulty of Ohmic loss in metals, Oulton et al. recently introduced the concept of a hybrid waveguide, consisting of a semiconductor nanowire (high-permittivity cylinder waveguide) separated from a metal surface by a nanoscale dielectric gap layer (essentially, an optical version of the MOS structure).[23] By optimization of the nanowire diameter and dielectric nanogap, the hybrid SPP/optical mode is strongly confined within the dielectric gap, allowing low-loss, deep-subwavelength confinement and long-range propagation of plasmonic fields.[19,23] Recently, this type of hybrid plasmonic structure has been applied to demonstrate plasmonic lasers in the waveguide,[19] total internal reflection,[20] or whispering-gallery configuration.[22] However, their physical sizes are still larger than

Received: July 2, 2011
Revised: August 29, 2011

dx.doi.org/10.1021/nl2022477 | *Nano Lett.* XXXX, XXX, 000–000

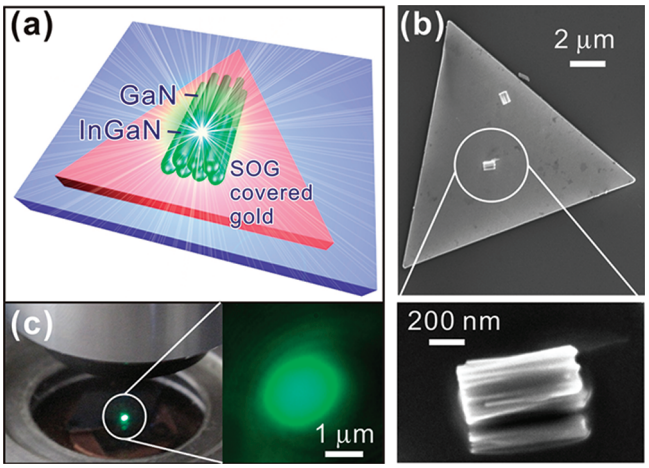

Figure 1. Plasmonic green nanolaser. (a) Schematic representation (not to scale) of the lasing MOS structure consisting of a bundle of green-emitting InGaN/GaN semiconductor nanorods, which is coupled to an underlying colloidal gold triangular plate through an SOG dielectric gap layer. The supporting substrate is silicon and the thickness of the SOG layer is about 5 nm. The average nanorod diameter is 30 nm, while the lengths of InGaN and GaN sections are 300 and 380 nm, respectively. (b) FE-SEM image of the hybrid system. The magnified image shows the detailed view of the measured InGaN/GaN nanorod bundle on top of the gold plate. From the FE-SEM image, we can estimate the 3D volume of the plasmonic "nanocapacitor" to be ~300 × 530 × 5 nm^3. (c) The green laser emission from the InGaN/SOG/gold hybrid system in a cyrostat (at 7 K) and under the excitation of a frequency-doubled Ti:sapphire laser system (excitation wavelength, 400 nm; pumping power density, 505 kW/cm^2).

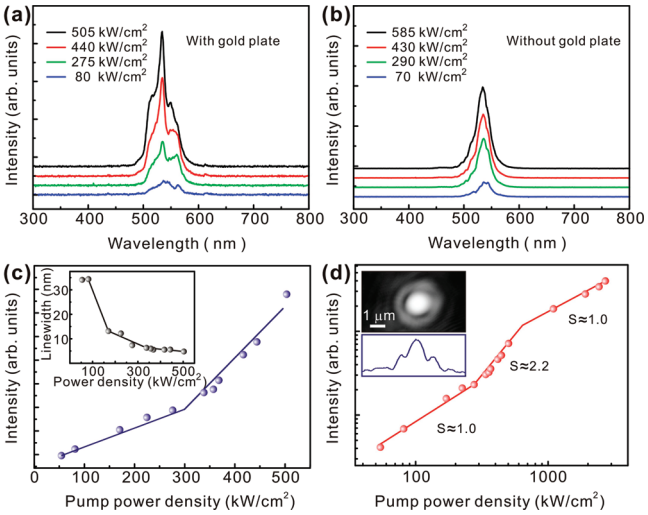

Figure 2. Lasing characteristics. (a) Power-dependent laser emission spectra of the InGaN/GaN nanorod bundle supported on the SOG-covered gold plate. These spectra were recorded at 7 K with varying excitation intensities, showing the transition from spontaneous emission to lasing at 533 nm. (b) In comparison, the power-dependent photoluminescence spectra of the InGaN/GaN nanorod bundle directly positioned on an SOG/Si substrate (without the gold plate) show no signs of lasing. For comparison, all emission spectra in (a) and (b) are plotted onto the same vertical scale. (c) For the lasing MOS structure, the superlinear response of the peak intensity becomes obvious when the excitation intensity is above the threshold intensity (~300 kW/cm^2). The inset shows the simultaneous line width narrowing of the emission peak above the lasing threshold. (d) The complete lasing characteristics are shown as a log−log plot together with the corresponding slopes (S) for different regions. The inset shows the defocused lasing mode image. The appearance of the high-contrast fringes indicates spatial coherence due to lasing.

the wavelength (greater than micrometers) in one or both lateral direction(s). To realize the 3D subdiffraction-limited lasers, we utilize here single-crystalline nitride semiconductor and gold building blocks, which are self-assembled materials with excellent optical/plasmonic and structural properties.[24−26] In addition, we demonstrate that this type of MOS structure can be applied for constructing single-mode plasmonic nanolasers in the green region, which has been urgently sought after due to a lack of efficient semiconductor gain medium.[27−29]

The InGaN/GaN semiconductor nanorod system utilized here has several advantages in terms of structural and thermal stability, amphoteric doping (for both n- and p-type GaN), as well as superior light emission properties for green and full-color (white) light-emitting devices.[25,30] Therefore, they are very suitable to be used as the gain medium in semiconductor nanolasers. In the blue spectral region, InGaN-quantum-well-based devices have high emission efficiencies. However, in the green and longer-wavelength spectral regions, their efficiencies dramatically drop, which has been known as the "green-gap" issue.[29] In order to design efficient InGaN-based light sources, different strategies have been developed in the past few years. One promising approach to modify the emission efficiency is the use of hybrid systems composed of noble metals and InGaN materials.[31,32] In comparison with sputtered Au or Ag films, we have found that colloidal Au nanocrystals possess superior plasmonic properties, allowing strong SPP-enhanced effects with a low Ohmic loss.[32]

Details about sample preparation procedures, as well as measurement and simulation methods for this study can be found in the Supporting Information. The self-aligned (along the c axis of the wurtzite structure), single-crystalline InGaN/GaN nanorods were grown on a Si(111) substrate by plasma-assisted molecular-beam epitaxy (PA-MBE) using a self-organized method without metal catalysts.[24] Figure 1a shows the schematic of the plasmonic nanolaser consisting of a green-emitting InGaN/GaN nanorod bundle coupled to a colloidal gold triangular plate with a 5 nm thick spin-on-glass (SOG, SiO_2) gap layer. The thickness of the colloidal gold plate is about 50 nm. The fabrication details for the MOS-structure-based plasmonic green nanolaser can also be found in Supporting Information. Figure 1b shows the field-emission scanning electron microscopy (FE-SEM) image of the measured plasmonic nanolaser structure. The InGaN/GaN nanorod bundle consists of several InGaN/GaN nanorods, and the average diameter of the nanorods is 30 ± 4 nm. The total length of the nanorod bundle is 680 nm (InGaN length, 300 nm; GaN length, 380 nm) and the bundle width is 530 nm. The self-aligned GaN nanorod array was grown first as the growth template for the subsequent InGaN nanorod growth. It should be noted that, according to a previous study, due to insufficient gain and large scattering at nanorod ends, these nanorods alone could not sustain laser oscillation under optical pumping unless their diameter is larger than 150 nm and their length is greater than a few micrometers.[5] Figure 1c shows an optical image of the laser emission at 533 nm from the InGaN/GaN nanorod bundle−gold plate hybrid system under the optical excitation of a frequency-doubled, mode-locked Ti:sapphire laser at 400 nm. In addition to the spatial overlap, the

dx.doi.org/10.1021/nl2022477 |Nano Lett. XXXX, XXX, 000–000

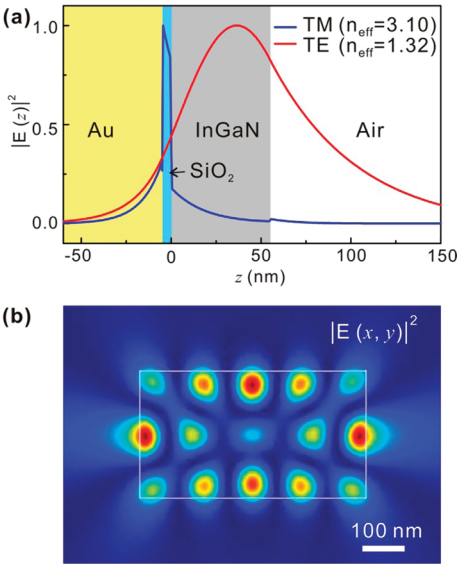

Figure 3. Simulations of the 1D + 2D mode distributions for the plasmonic cavity mode at 533 nm. (a) The electric-field-intensity distributions along the z (vertical) direction for both the TM and TE polarizations. Only the TM mode shows strong confinement in the SiO_2 gap layer, while the TE mode extends into the metal, semiconductor, and air regions. (b) The electric-field-intensity (TM polarization) distribution in the x and y (lateral) directions, illustrating the 2D mode confinement in the SiO_2 gap region sandwiched between the InGaN nanorod bundle (rectangular region 530 × 300 nm^2) and the Au layer. The calculated quality factor (Q) is 93, which is very close to the experimental value of ~100.

plasmon coupling critically depends on the spectral overlap of surface plasmon resonance band with the light emission peak of the gain medium. In Supporting Information, we show that the surface plasmon resonance band of the gold triangular plate indeed overlaps with the luminescent emission peak of the InGaN/GaN nanorods at 7 K. However, the spectral match is not completely optimized due to the trade-off of using the colloidal gold nanocrystal for their superior material properties.

Figure 2a presents excitation-power-dependent emission spectra from the InGaN/GaN nanorod bundle deposited on an SOG-covered gold plate at a cryogenic temperature (7 K). These spectra were measured for the same hybrid system presented in Figure 1b. At low pump power density (80 kW/cm^2), we observed a relatively broad spontaneous emission peak centered at 540 nm. As the pump power density is increased, the peak emission rapidly increases its intensity and becomes more dominant. Above a threshold of 300 kW/cm^2, a sharp lasing peak emerges in the spectra at 533 nm. The full width at half-maximum (fwhm) of the observed laser emission peak at the pumping power density of 505 kW/cm^2 is 4.7 nm. In contrast, for the bare InGaN/GaN nanorod bundle (a control sample, which was directly supported on an SOG/Si substrate without the presence of the gold plate; in Supporting Information, we also show a similar result for an InGaN/GaN nanorod bundle deposited on a quartz substrate), the power-dependent photoluminescence (PL) spectra displayed in Figure 2b show no sign of lasing. Instead, we observed a linear dependence of the PL emission intensity as well as a constant fwhm. The power dependence of the laser emission intensity shown in Figure 2a is summarized in Figure 2c, which clearly shows that above the threshold excitation intensity, a nonlinear dependence of the

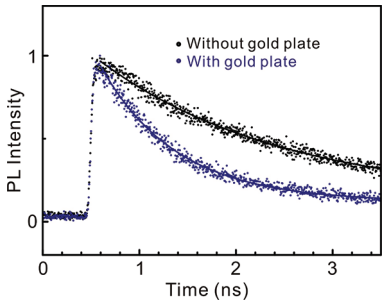

Figure 4. Enhanced spontaneous emission rate. Time-resolved spontaneous emission at 7 K under weak pumping conditions shows a reduction in lifetime for the InGaN/GaN nanorod bundle positioned on an SOG-covered gold plate. The measured lifetime of the InGaN/GaN nanorod bundle directly positioned on an SOG/Si substrate is 1.9 ns, while the measured lifetime of InGaN/GaN nanorod bundle on gold plate is 0.8 ns. The reduction in lifetime is due to the Purcell effect.

emission intensity starts to appear. Also shown in Figure 2c, the superlinear dependence of the emission intensity and the line width narrowing at high pumping power happen concomitantly, indicating a transition from spontaneous to amplified and stimulated emissions. In Figure 2d, we present the log−log plot of the same data set as in Figure 2c. The S-shaped curve clearly shows the transition from spontaneous emission (S = 1) to amplified spontaneous emission (S > 1) and finally into the lasing regime (S = 1). The inset in Figure 2d displays an optical image of the defocused emitted beam above the lasing threshold. In this image, circular fringes around the laser emission spot can be observed, indicating strong spatial coherence. Similar patterns for semiconductor nanolasers excited above the lasing threshold have also been reported.[10,33] This observation is another indication of lasing (spasing) phenomenon for this plasmonic nanolaser.

To understand the 3D mode distributions for the studied structure, numerical simulations were performed to calculate the electric-field-intensity distributions using the combined 1D eigenmode and 2D finite-difference time-domain (FDTD) methods (1D + 2D; see, e.g., ref 20). Figure 3a shows the 1D mode distributions for both the TM mode (transverse magnetic; the electric-field component is perpendicular to metal surface) and the TE mode (transverse electric; the electric-field component is parallel to metal surface) along the z direction at the lasing (spasing) wavelength of 533 nm. In this simulation, the TM mode shows strong confinement in the SiO_2 gap with low metal loss (it should be noted that there is still some tail coupling with the semiconductor region to facilitate the required optical pumping of the InGaN gain medium). In contrast, the TE mode is quite delocalized. We confirm that only the TM mode can have a sufficiently large momentum (effective indices, n_{eff} = 3.10 (TM) and n_{eff} = 1.32 (TE)) to hybridize with SPPs and form the plasmonic cavity mode, providing the necessary cavity feedback mechanism for lasing (spasing). In a recent theoretical study,[34] it has been pointed out that giant gain exists near the SPP resonance where the maximal wavelength compression (effective index) enables the slowing down of energy propagation and a highly localized field distribution. For the present case, this peculiar feature in plasmonic nanocavities allows the subdiffraction-limited nanolaser operation despite a large radiation loss.

Furthermore, the electric field distribution of TM mode in the x and y (lateral) directions was investigated (Figure 3b),

dx.doi.org/10.1021/nl2022477 |Nano Lett. XXXX, XXX, 000–000

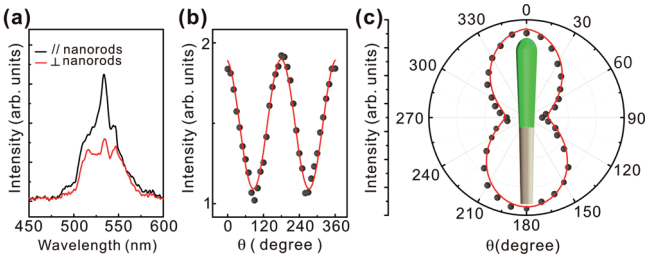

Figure 5. Anisotropic laser emission. (a) Variation of laser emission intensity with two different polarizer orientations. These spectra were recorded with the emission polarization oriented parallel (black curve) and perpendicular (red curve) to the nanorod axis (the *c* axis of the wurtzite crystal structure). The measured polarization ratio is 0.3. (b, c) Plots of laser emission at 7 K as a function of the emission polarization angle relative to the nanorod axis. The filled circles represent the measured data points and the solid lines are the fitting curves.

confirming the strong 2D confinement in this plasmonic laser structure. The calculated quality factor (Q) is 93, which is very close to the experimental value (~100). Supported by the simulation results, the mode volume for this plasmonic laser can be estimated to be $8.0 \times 10^{-4} \mu m^3$ ($\sim 0.14(\lambda/2n)^3$), which is smaller than the previously reported mode volumes in the literature. In addition, we have simulated the spectral positions of the cavity eigenmodes using the 1D + 2D approach. The resulting spectral structure is in good agreement with that shown in Figure 2a. It should be emphasized that the shape of the nanorod bundle, rather than the shape of the colloidal gold plate, determines the observed spectral structure. In the Supporting Information, we present a similar lasing phenomenon from an InGaN/GaN nanorod bundle deposited on a colloidal gold hexagonal plate.

The SPP coupling behavior was also observed by low-temperature, time-resolved PL measurements under weak pumping conditions. Under these conditions, the heating and exciton−exciton scattering effects can be avoided.[20] Figure 4 presents the temporal profiles of the PL intensity from the InGaN/GaN nanorod bundle supported on an SOG-covered gold plate (blue line) and on an SOG/Si substrate (black line), respectively. A pronounced decrease in PL decay lifetime is observed (from 1.9 to 0.8 ns), judging by measurements from the bare InGaN/GaN nanorod bundle (deposited on SOG/Si) and the InGaN/GaN nanorod bundle−SOG−gold plate at the peak emission wavelength. It should be noted that, to rule out the possible effects of leaky mode into the high-refractive-index Si substrate, we have also performed a control experiment on a transparent (low-refractive-index) quartz substrate. The measured PL decay lifetime was confirmed to be identical to that using the SOG/Si substrate (shown in the Supporting Information). It has been suggested that reduction of PL decay lifetime is closely related to the Purcell effect of plamonic nanocavity due to the spatial proximity and close spectral match between the excitons in semiconductor and the SPPs excited in metal.[20] As a result of exciton−plasmon coupling, the PL decay lifetime is significantly shortened. These measurement results reveal that the SPPs confined in the SiO_2 nanogap layer can indeed provide the coherent feedback mechanism for the plasmonic laser structure.

However, although comparable with the reported values for plamonic nanocavities,[19,21] the measured Purcell factor (~2.5) is relatively low in comparison with the conventional case of dielectric or semiconductor cavities. One way to enhance the Purcell factor is to utilize high-quality colloidal silver nanocrystals for a better SPP spectral match with the present InGaN gain medium. As mentioned above, in this experiment, we adopted the colloidal gold nanocrystal for their superior material properties.

Because the InGaN/GaN nanorods have a highly anisotropic structure, we have also measured the existence of laser emission anisotropy using a normal incident/collection measurement geometry. Figure 5a shows the polarized laser emissions from the InGaN/GaN nanorods bundle−SOG−gold plate hybrid system with the electric field of luminescence oriented parallel and perpendicular to the nanorod axis (the *c* axis of the wurtzite crystal structure), respectively. The polarized emission signal was measured by using a polarizer positioned in the emission collection pathway. We found that the intensity of polarized emission with the electric field parallel to the nanorods axis is much larger than that perpendicular to the nanorods axis. The observed polarization anisotropy is typically defined in terms of the polarization ratio $\rho = (I_{\parallel} - I_{\perp})/(I_{\parallel} + I_{\perp})$.[35] The measured polarization ratio is ~0.3. Figure 5b shows that the emission exhibits a clear modulation with continuously varying polarization orientations. In Figure 5c, we present a polar plot of laser emission as a function of the emission polarization angle relative to the long axis of nanorods axis. The mechanism of the observed polarized emission might result from anisotropic gain medium (shape anisotropy),[35] optical confinement effect (subwavelength nanorod cavity),[36] intrinsic nanomaterial property,[37] or combination of the above effects. A further study is required to clarify the underlying mechanism.

In summary, we have demonstrated that the MOS-based plasmonic laser can be operated in a 3D subdiffraction-limited regime. By use of the MOS-based structure, the highly pursued green semiconductor nanolaser can be realized with enhanced emission properties. Since the GaN semiconductor could be doped with both n- and p-types, an electrically injecting version might become feasible in the near future. The implementation of this type of InGaN plasmonic nanolaser operating well below the diffraction limit can find a wide range of applications for optical integrated circuits, ultrahigh-density optical data storage, ultrafast optical communication, as well as biological/chemical sensing and imaging in the visible and infrared spectral regions.

■ ASSOCIATED CONTENT

Ⓢ Supporting Information. Details of sample growth and preparation procedures, optical measurement setups, numerical simulation method, as well as additional experimental data. This material is available free of charge via the Internet at http://pubs.acs.org.

■ AUTHOR INFORMATION

Corresponding Author

*E-mail: gwo@mx.nthu.edu.tw, hyahn@mail.nctu.edu.tw.

■ ACKNOWLEDGMENT

This work was supported in part by the National Science Council, Taiwan through the National Nanoscience and Nanotechnology Program (Grant No. NSC-99-2120-M-007-004) and a research project (Grant No. NSC-98-2112-M-009-MY3).

dx.doi.org/10.1021/nl2022477 |*Nano Lett.* XXXX, XXX, 000–000

REFERENCES

(1) McCall, S. L.; Levi, A. F. J.; Slusher, R. E.; Pearton, S. J.; Logan, R. A. *Appl. Phys. Lett.* **1992**, *60*, 289–291.

(2) Huang, M. H.; Mao, S.; Feick, H.; Yan, H.; Wu, Y.; Kind, H.; Weber, E.; Russo, R.; Yang, P. *Science* **2001**, *292*, 1897–1899.

(3) Duan, X.; Huang, Y.; Agarwal, R.; Lieber, C. M. *Nature* **2003**, *421*, 241–245.

(4) Qian, F.; Li, Y.; Gradečak, S.; Park, H.-G.; Dong, Y.; Ding, Y.; Wang, Z. L.; Lieber, C. M. *Nat. Mater.* **2008**, *7*, 701–706.

(5) Zimmler, M. A.; Bao, J.; Capasso, F.; Müller, S.; Ronning, C. *Appl. Phys. Lett.* **2008**, *93*, 051101.

(6) Painter, O.; Lee, R. K.; Scherer, A.; Yariv, A.; O'Brien, J. D.; Dapkus, P. D.; Kim, I. *Science* **1999**, *284*, 1819–1821.

(7) Matsubara, H.; Yoshimoto, S.; Saito, H.; Jianglin, Y.; Tanaka, Y.; Noda, S. *Science* **2008**, *319*, 445–447.

(8) Tandaechanurat, A.; Ishida, S.; Guimard, D.; Nomura, M.; Iwamoto, S.; Arakawa, Y. *Nat. Photonics* **2011**, *5*, 91–94.

(9) Hill, M. T.; Oei, Y.-S.; Smalbrugge, B.; Zhu, Y.; de Vries, T.; van Veldhoven, P. J.; van Otten, F. W. M.; Eijkemans, T. J.; Turkiewicz, J. P.; de Waardt, H.; Geluk, E. J.; Kwon, S.-H.; Lee, Y.-H.; Nötzel, R.; Smit, M. K. *Nat. Photonics* **2007**, *1*, 589–594.

(10) Nezhad, M. P.; Simic, A.; Bondarenko, O.; Slutsky, B.; Mizrahi, A.; Feng, L.; Lomakin, V.; Fainman, Y. *Nat. Photonics* **2010**, *4*, 395–399.

(11) Yu, K.; Lakhani, A.; Wu, M. C. *Opt. Express* **2010**, *18*, 8790–8799.

(12) Barnes, W. L.; Dereux, A.; Ebbesen, T. W. *Nature* **2003**, *424*, 824–830.

(13) Gramotnev, D. K.; Bozhevolnyi, S. I. *Nat. Photonics* **2010**, *4*, 83–91.

(14) Schuller, J. A.; Barnard, E. S.; Cai, W.; Jun, Y. C.; White, J. S.; Brongersma, M. L. *Nat. Mater.* **2010**, *9*, 193–204.

(15) Stockman, M. I. *Phys. Today* **2011**, *64*, 39–44.

(16) Bergman, D. J.; Stockman, M. I. *Phys. Rev. Lett.* **2003**, *90*, 027402.

(17) Stockman, M. I. *J. Opt.* **2010**, *12*, 024004.

(18) Zheludev, N. I.; Prosvirnin, S. L.; Papasimakis, N.; Fedotov, V. A. *Nat. Photonics* **2008**, *2*, 351–354.

(19) Oulton, R. F.; Sorger, V. J.; Zentgraf, T.; Ma, R.-M.; Gladden, C.; Dai, L.; Bartal, G.; Zhang, X. *Nature* **2009**, *461*, 629–632.

(20) Ma, R.-M.; Oulton, R. F.; Sorger, V. J.; Bartal, G.; Zhang, X. *Nat. Mater.* **2011**, *10*, 110–113.

(21) Noginov, M. A.; Zhu, G.; Belgrave, A. M.; Bakker, R.; Shalaev, V. M.; Narimanov, E. E.; Stout, S.; Herz, E.; Suteewong, T.; Wiesner, U. *Nature* **2009**, *460*, 1110–1112.

(22) Kwon, S.-H.; Kang, J.-H.; Seassal, C.; Kim, S.-K.; Regreny, P.; Lee, Y.-H.; Liber, C. M.; Park, H.-G. *Nano Lett.* **2010**, *10*, 3679–3683.

(23) Oulton, R. F.; Sorger, V. J.; Genov, D. A.; Pile, D. F. P.; Zhang, X. *Nat. Photonics* **2008**, *2*, 496–500.

(24) Chen, H.-Y.; Lin, H.-W.; Shen, C.-H.; Gwo, S. *Appl. Phys. Lett.* **2006**, *89*, 243105.

(25) Hong, C.-C.; Ahn, H.; Wu, C.-Y.; Gwo, S. *Opt. Express* **2009**, *17*, 17227–17233.

(26) Ditlbacher, H.; Hohenau, A.; Wagner, D.; Kreibig, U.; Rogers, M.; Hofer, F.; Aussenegg, F. R.; Krenn, J. R. *Phys. Rev. Lett.* **2005**, *95*, 257403.

(27) Nakamura, S.; Riordan, M. *Sci. Am.* **2009**, *300*, 70–75.

(28) Enya, Y.; Yoshizumi, Y.; Kyono, T.; Akita, K.; Ueno, M.; Adachi, M.; Sumitomo, T.; Tokuyama, S.; Ikegami, T.; Katayama, K.; Nakamura, T. *Appl. Phys. Express* **2009**, *2*, 082101.

(29) Ohta, H.; DenBaars, S. P.; Nakamura, S. *J. Opt. Soc. Am. B* **2010**, *27*, B45–B49.

(30) Lin, H.-W.; Lu, Y.-J.; Chen, H.-Y.; Lee, H.-M.; Gwo, S. *Appl. Phys. Lett.* **2010**, *97*, 073101.

(31) Okamoto, K.; Niki, I.; Shvartser, A.; Narukawa, Y.; Mukai, T.; Scherer, A. *Nat. Mater.* **2004**, *3*, 601–605.

(32) Wu, C.-Y.; He, C.-L.; Lee, H.-M.; Chen, H.-Y.; Gwo, S. *J. Phys. Chem. C* **2010**, *114*, 12987–12993.

(33) van Vugt, L. K.; Rühle, S.; Vanmaekelbergh, D. *Nano Lett.* **2006**, *6*, 2707–2711.

(34) Li, D. B.; Ning, C. Z. *Appl. Phys. Lett.* **2010**, *96*, 181109.

(35) Wang, J.; Gudiksen, M. S.; Duan, X.; Cui, Y.; Lieber, C. M. *Science* **2001**, *293*, 1455–1457.

(36) Chen, H.-Y.; Lin, H.-W.; Wu, C.-Y.; Chen, W.-C.; Chen, J.-S.; Gwo, S. *Opt. Express* **2008**, *16*, 8106–8116.

(37) Lu, Y.-J.; Lin, H.-W.; Chen, H.-Y.; Yang, Y.-C.; Gwo, S. *Appl. Phys. Lett.* **2011**, *98*, 233101.